Transport Properties of Tetrahedral, Network-Forming Ionic Melts

Manish Agarwal, Abir Ganguly, and Charusita Chakravarty*

Department of Chemistry, Indian Institute of Technology-Delhi, New Delhi: 110016, India

Received: April 22, 2009; Revised Manuscript Received: September 2, 2009

Molecular dynamics simulations of liquid silica and beryllium fluoride are performed using the van Beest−Kramer−van Santen and transferable rigid ion model potentials, respectively, in order to compare transport properties. The ionic conductivity (σ), shear viscosity (η) and ionic self-diffusivities ($D_{\pm}$) are computed over a fairly wide range of temperatures and densities and deviations from Arrhenius behavior along different isochores is studied. The Stokes−Einstein relation is shown to hold over the entire range of state points, though the effective hydrodynamic radius shows small variations due to thermal fluctuations, compression, and local tetrahedral order. Several alternative tests of the Nernst−Einstein relation are implemented which show that significant network-formation in the anomalous regime leads to a breakdown of this relationship. The relaxation times, τ_σ and τ_M, associated with the decay of the charge-flux and pressure ACFs respectively, are computed. In the anomalous regime, as the tetrahedral network formation progresses, τ_M increases rapidly while τ_σ shows very little variation, indicating a decoupling of charge and momentum transport processes.

1. Introduction

Quantitative relationships between structural, thermodynamic, and dynamic properties are valuable for understanding and predicting properties of complex fluids. Ionic melts represent an interesting category of liquids that may be thought of as a multicomponent mixture of atoms with very different electronegativities. If the electronegativity difference is large, then coulombic interactions dominate structure, as in alkali halides, and the corresponding molten salts can be regarded as simple liquids.[1] As the electronegativity difference decreases, however, local anisotropic or "covalent" interactions result in formation of complex, network-forming liquids, e.g., molten BeF_2, SiO_2, or $AlCl_3$. The complex interplay of relative electronegativities and polarizabilities results in a diversity of liquid state structures, anomalous properties, and polyamorphic phases, many of which have significant technological applications.[2,3]

This study focuses on transport properties of AB_2 ionic melts which form three-dimensional, locally tetrahedral networks similar to the hydrogen-bonded network of water. Examples of such ionic melts are SiO_2,[4−14] BeF_2,[15−22] $ZnCl_2$,[23−25] and GeO_2.[26,27] In the case of molten silica and beryllium fluoride, the presence of a three-dimensional, tetrahedral liquid-state network has been shown to be associated with water-like thermodynamic and kinetic anomalies.[5,7,28−33] Like water and mesoscopic liquids with core-softened potentials, these ionic melts show a density anomaly, where density increases on isobaric heating, and a diffusional anomaly, where diffusivity increases on isothermal compression. Since these liquids undergo a transition from a normal to an anomalous regime as a function of temperature or density, they are convenient systems to understand how structural changes are connected with modifications of equilibrium thermodynamic or transport properties.

A quantitative framework for understanding the relationship between structural order and liquid-state anomalies in tetrahedral, network-forming liquids was originally developed by Errington and Debenedetti for water.[32] They used a tetrahedral order parameter, q_{tet} to measure the degree of local orientational order around a tetrahedral center (e.g., O in H_2O and Be in BeF_2). A translational order parameter, τ, was defined to measure the extent short-range order induced by pair correlations between tetrahedral centers. It was shown that for low-temperature isotherms, q_{tet} has a maximum and τ has a minimum as a function of density; the loci of these extrema in the order define a structurally anomalous region in the density−temperature (ρT) plane within which q_{tet} and τ are strongly correlated. The region of the density anomaly, where $(\partial\rho/\partial T)_P > 0$, is bound by the structurally anomalous region. The diffusionally anomalous region ($(\partial D/\partial\rho)_T > 0$) closely follows the boundaries of the structurally anomalous region, specially at low temperatures. In water, the structurally anomalous region encloses the region of anomalous diffusivity. The nested structure of regions corresponding to structural, diffusional, and density anomalies is now regarded as a defining feature of liquids with water-like anomalies, including the ionic melts discussed here as well as mesoscopic, core-softened fluids.

An alternative approach to developing quantitative connections between mobility and structure of liquids can be developed using the excess entropy (S_e), defined as the difference between the total thermodynamic entropy (S) and the corresponding ideal gas entropy (S_{id}) at the same temperature and density.[34−44] The excess entropy represents the lowering of the entropy of a fluid due to the presence of static structural correlations of the fluid. Formally, this can be expressed as a multiparticle correlation expansion, $S_e = S_2 + S_3 + \cdots$, where S_n is the entropy contribution due to n particle spatial correlations.[45−47] The pair correlation contribution is typically the dominant contribution to the excess entropy of simple liquids, molecular fluids, such as water, and ionic melts. The excess entropy can also be related to transport properties using scaling relationships of the form: $X^* = A \exp(\alpha S_e)$ where X^* are dimensionless transport properties with either macroscopic (Rosenfeld) or microscopic (Dzugutov) reduction parameters.[38,48−50] The scaling form may be justified using corresponding states arguments or mode-coupling theory.[50,51] Intuitively, the scaling relationships reflect

* To whom correspondence should be addressed. Tel: (+)91-11-2659-1510. Fax: (+)91-11-2686-2122. E-mail: charus@chemistry.iitd.ernet.in.

10.1021/jp903694b CCC: $40.75
Published on Web 10/27/2009

the fact that structural correlations lower the excess entropy as well as the single-particle mobility by enhancing cage effects due to nearest neighbor shells. While entropy scaling relationships for transport properties were originally formulated for simple liquids, they have been used very successfully in recent work to connect structure, mobility, and entropy in liquids with waterlike anomalies,[35−39] confined fluids,[40] and polymeric melts.[41] In particular, the existence of water-like thermodynamic and diffusional anomalies in systems as different as tetrahedral ionic melts and colloidal fluids with core-softened interactions can be explained as due to the presence of an excess entropy anomaly, corresponding to an increase in excess entropy on isothermal compression ($(\partial S_e/\partial \rho)_T > 0$). On thermodynamic grounds, the excess entropy anomaly will be associated with density, compressibility, and heat capacity anomalies.[28] Since diffusivities in both the tetrahedral ionic melts as well as core-softened fluids obey Rosenfeld-type scaling relationships, the excess entropy anomaly will be associated with the diffusional anomaly. The structural origins of the excess entropy anomaly in tetrahedral liquids and core-softened isotropic fluids lie in a density-driven change in the nature of local order. In the case of tetrahedral liquids, the short-range orientational order shifts from tetrahedral at low densities to random close-packed order at high densities, giving rise to an excess entropy maximum at intermediate densities. In the case of core-softened fluids, the excess entropy anomaly originates in the competition between two different length scales as a function of density.[35−39,42−44]

A recent study considers the relationships between structure, entropy, and three different mobility measures (diffusivity, viscosity, and ionic conductivity) in tetrahedral ionic melts using molecular dynamics simulations of BeF_2 and SiO_2.[52] The validity of the Nernst−Einstein and the Stokes−Einstein equations, which relate the ionic conductivity and viscosity respectively to the diffusivity, was examined since deviations from these relations would signal that relaxation processes associated with the different dynamical properties are not the same. The Stokes−Einstein relationship connecting ionic diffusivities with the viscosity was found to be valid and both molten BeF_2 and SiO_2 displayed a water-like viscosity anomaly, in addition to the diffusional anomaly. In contrast, within the structurally anomalous region,[32] a striking breakdown of the Nernst−Einstein relation was observed. In order to understand the connection between structure and dynamics, the scaling of the different transport properties with the total excess entropy as well as the different pair correlation entropy contributions was considered. The ionic diffusivities ($D_\pm$) as well as viscosity (η) for both the ionic melts showed similar Rosenfeld-scaling with the excess entropy (S_e), as well as with the dominant pair correlation contribution (S_2), e.g., $\ln D_+ \propto S_2$. In contrast to the diffusivity and viscosity, the ionic conductivity (σ) displayed exponential scaling with only the cation−anion contribution to the pair correlation entropy, e.g., $\ln \sigma^* \propto S_{AB}$.

The present study was undertaken as an extension of our earlier work[52] in order to understand the dramatic breakdown of the Nernst−Einstein equation and the unexpected and qualitatively different behavior of the viscosity and conductivity with regard to excess entropy scaling. A detailed comparison of the transport properties of liquid silica and beryllium fluoride using the van Beest−Kramer−van Santen (BKS) and transferable rigid ion model (TRIM) potentials is respectively presented.[52] The ionic conductivity (σ), shear viscosity (η) and ionic self-diffusivities ($D_\pm$) are studied over a fairly wide range of temperatures and densities so that relationships between the transport properties can be examined for the ionic melts in the normal and anomalous regimes. Deviations from Arrhenius behavior along different isochores is mapped out. Alternative tests for Stokes−Einstein and Nernst−Einstein behavior are considered and the relaxation times associated with the pressure and charge-flux autocorrelation functions are computed.

2. Computational Details

We use the transferable rigid ion model (TRIM) potential for BeF_2, modeling electrostatic long-range interactions with coulomb interactions and short-range repulsions using a Born−Mayer−Huggins parametric form. The pair interaction between ions i and j is given by the the following:

$$\phi_{TRIM}(r_{ij}) = \frac{z_i z_j e^2}{4\pi\varepsilon_0 r_{ij}} + \left(1 + \frac{z_i}{n_i} + \frac{z_j}{n_j}\right) \times b \exp\left(\frac{\sigma_i + \sigma_j - r_{ij}}{s}\right) \quad (1)$$

where r_{ij} is the distance between atoms i and j. The parameters associated with an atom of type l are the charge z_l, the number of valence-shell electrons n_l and the ionic size parameter σ_l. The repulsion parameter b and the softness parameter s are assumed to be the same for all three types of pair interactions. All three pairs of interactions are considered for the parametrization.[9,7,42,53]

To model the interatomic interactions in silica, we use the van Beest−Kramer−van Santen (BKS) potential with an additional 30−6 Lennard−Jones type correction term.[11,54,55] The pair interaction between atoms i and j is given by the following:

$$\phi_{BKS}(r_{ij}) = \frac{q_i q_j}{4\pi\varepsilon_0 r_{ij}} + A_{ij} \exp^{-b_{ij} r_{ij}} - \frac{C_{ij}}{r_{ij}^6} + 4\varepsilon_{ij}\left[\left(\frac{\sigma_{ij}}{\Gamma_{ij}}\right)^{30} - \left(\frac{\sigma_{ij}}{\Gamma_{ij}}\right)^{6}\right] \quad (2)$$

where r_{ij} is the distance between atoms i and j carrying charges q_i and q_j, A_{ij}, b_{ij} and C_{ij} are the parameters associated with the Buckingham potential for short-range repulsion-dispersion interactions and ε_{ij} and σ_{ij} are the energy and length scale parameters for the 30−6 Lennard−Jones interaction. The parameters for the modified BKS potential used in this work are given ref 56.

Molecular dynamics (MD) simulations of BeF_2 and SiO_2 melts were performed in the canonical (NVT) ensemble. In all simulations, the leapfrog Verlet integration scheme with a time step of 1 fs was used, as implemented in the DL_POLY simulation package.[7,17,54,57] The simulation box contains 150 positive (Be or Si) and 300 negative (F or O) ions. Ewald summation was used to estimate Coulombic contribution to the potential. Temperature was maintained using the Berendsen thermostat, with a time constant of $\tau_B = 200$ ps. This large value of the time constant was chosen to minimize any perturbation of the intrinsic dynamics of the systems. Tests with for τ_B lying between 1 and 200 ps at selected state points did not, however, display any significant variations. To evaluate the thermodynamic excess entropy, a thermodynamic integration procedure originally developed for SiO_2 was used.[5,6] The computational procedure used to by us to estimate the excess entropy of BeF_2 and SiO_2 is discussed in detail in ref 44.

Diffusivities were evaluated using the Einstein relation and the shear viscosity and ionic conductivity were evaluated using the Green−Kubo route.[1,58] For BeF_2, statistics were collected

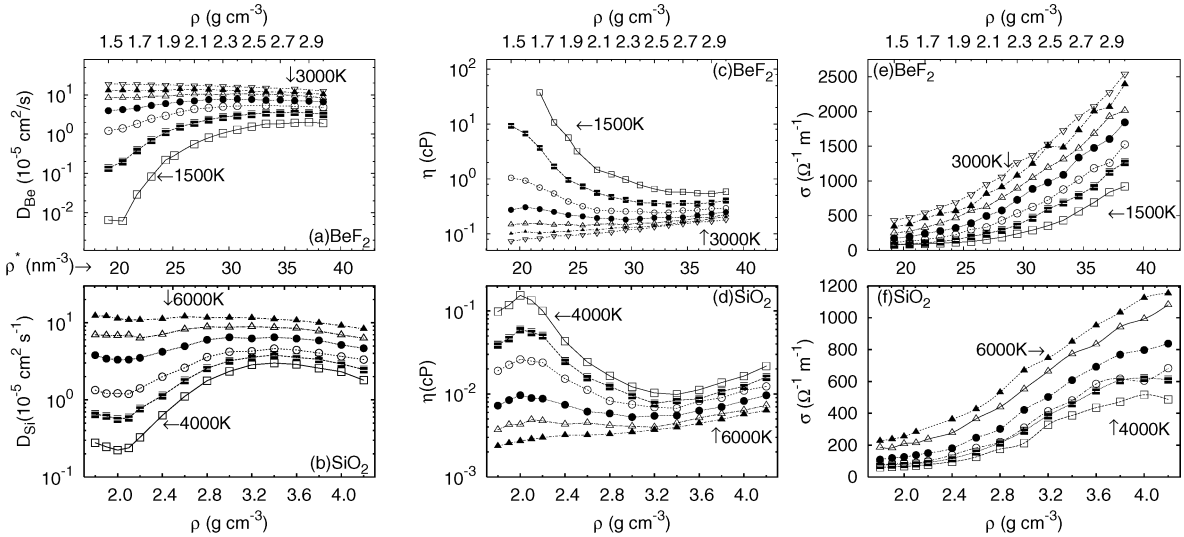

Figure 1. Behavior of transport quantities as a function of density (ρ) along different isotherms. The top row shows the (a) cationic self-diffusivity, D_+, (c) the shear viscosity, η and (e) the ionic conductivity, σ for BeF_2. The bottom row, i.e., parts (b), (d), and (f) show the corresponding quantities for SiO_2. The key labels of the isotherms for BeF_2 are 1500 K (□), 1750 K (■), 2000 K (○), 2250 K (●), 2500 K (Δ), 2750 K (▲), and 3000 K (∇). Isotherms for SiO_2 are labeled as 4000 K (□), 4250 K (■), 4500 K (○), 5000 K (●), 5500 K (Δ), and 6000 K (▲). Densities in g cm^{-3} are given along the lower x-axis for SiO_2 and the upper x-axis for BeF_2. The number density (in nm^{-3}) is given in the middle of the upper and lower plots in each column. Note the logarithmic scale on the y-axis for D_A and η.

over 6 ns for high temperatures ($T > 2250$ K) and 8 ns for low temperatures ($T \leq 2250$ K). Configurations were stored every 500 fs and pressure tensor (corresponding to the negative of the stress tensor) was stored every 2−5 steps for estimation of diffusivities and viscosity, respectively.[59,60] Separate short runs of 2 ns were done with ion flux data stored every step for calculation of conductivities. Note that the runs for estimating conductivity are somewhat longer than the 0.5 ns runs used in our previous studies.[52,58] For SiO_2, all production runs were 8 ns, with pressure tensor and ion flux data stored every step. The configurations were stored every 500 fs. For all diffusivity and viscosity estimations, the trajectories were split into 1 ns non-overlapping sections, and the resulting values averaged. The errors in transport properties were at most of the order of 1−5%, except at the lowest densities for the lowest isotherms, where slow equilibration reduces statistical certainty.

3. Results and Discussion

3.1. Density and Temperature Dependence of Transport Properties. Thermodynamic and structural anomalies of both BeF_2 and SiO_2 have been previously mapped out.[7,42,43] The region of density anomaly is bounded by the locus of state points for which $(\partial\rho/\partial T)_P = 0$, corresponding to temperatures of maximum or minimum density along an isobar. The state point corresponding to the maximum temperature along this locus indicates the highest temperature for which thermodynamic anomalies can be observed. This state point, denoted by (T^{max}_{TMD}, ρ^{max}_{TMD}), occurs at (5000 K, 2.3 g cm^{-3}) for SiO_2 and (2310 K, 1.8 g cm^{-3}) for BeF_2.[7,42] The value of ρ^{max}_{TMD} for both SiO_2 and BeF_2 corresponds to the same number density of 23.07 nm^{-3}, indicating the structural similarities in the melts.

Figure 1 shows the density dependence of diffusivity, viscosity and conductivity along different liquid state isotherms of BeF_2 and silica. Both of the melts show show viscosity (η) and diffusivity ($D_\pm$) anomalies, as expected on the basis of earlier studies.[5,7,10,17,29,32,42−44] The maxima in the cationic diffusivity (D_+) and the viscosity (η) occur at essentially the same number density for both the melts. This suggests the possibility of corresponding states relationships between tetrahedral liquids, provided appropriate reduced units are used.[52] The region of diffusional anomaly on the temperature-density plane is bounded by the locus of extrema in the $D(\rho)$ curves along different isotherms. Diffusivity minima (alternatively, maxima in $\eta(\rho)$) can be located along isotherms at temperatures of 5000 K or less for SiO_2 and only for the 1500 K isotherm for BeF_2. The boundaries for the regions of these two mobility anomalies constructed from our data suggest that the region of viscosity anomaly is located within that of the diffusivity, as seen in simple liquids.[39]

In contrast to the behavior of diffusivity and viscosity, the conductivity shows a monotonic rise with compression for all of the isotherms studied here. It would appear that compression destroys the network and facilitates conductivity over the density range studied here. Note that in BeF_2, while viscosities and diffusivities vary over 3 orders of magnitude, the conductivity varies over a couple of orders of magnitude. In the case of SiO_2, the difference in range of variation of conductivity and viscosity is less pronounced. We note that decrease in diffusivity with compression sets in only for number densities greater than 34 nm^{-3}. It is possible that at densities greater than this, steric effects would become dominant and a substantial decrease in diffusivity would also result in a lowering of ionic conductivity, as is seen in the 4000 K isotherm of SiO_2 shown in Figure 1(f).

Figure 2 shows the dependence of $\ln(\eta)$ as a function of $1/T$ for BeF_2 and SiO_2. Figure 3 plots the temperature dependence of the conductivity as a function of $1/T$. Tables 1 and 2 provide the details of the fitting of viscosity and conductivity data to the Arrhenius equation for BeF_2 and SiO_2, respectively.

We first consider the validity of the Arrhenius relationship for the viscosity. In the case of BeF_2, for isochores corresponding to densities of 2.0 g cm^{-3} or greater, the viscosity data for the temperature range from 1500 K to 3000 K can be fitted to the form $\ln \eta = 1000 m_\eta/T + c$ with a 2−5% error in the density-dependent slopes. For lower densities, the temperature range over which we could fit the data with similar % error was smaller. The results for the viscosity of liquid SiO_2 are qualitatively similar. The viscosity data for isochores with densities of 3 g cm^{-3} or more can be fitted to the Arrhenius

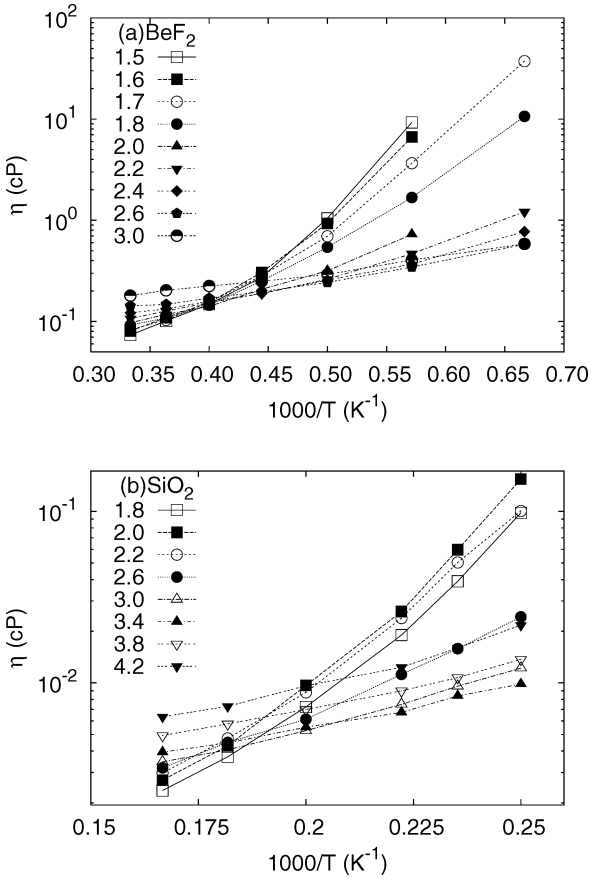

Figure 2. Viscosity (η) as a function of reciprocal temperature for (a) BeF_2 and (b) SiO_2 with logarithmic scale on y-axis.

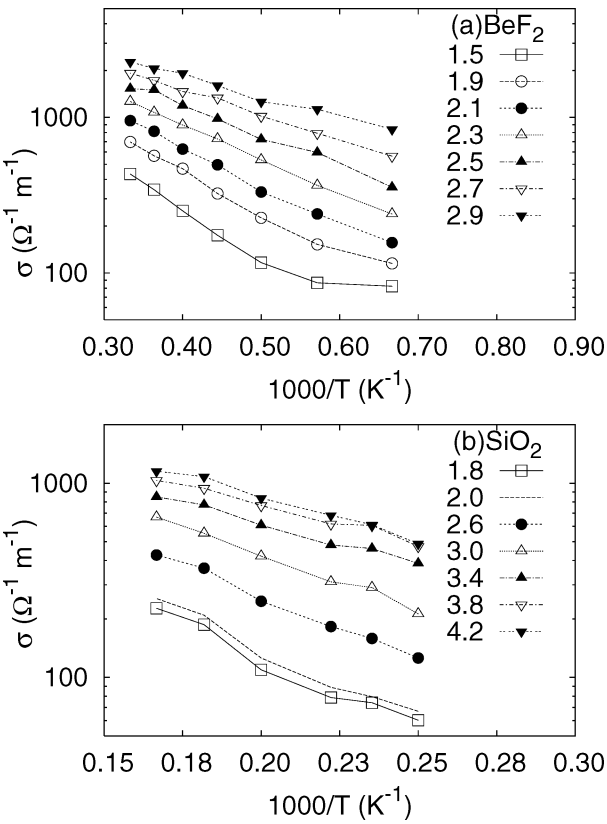

Figure 3. Conductivity (σ) as a function of reciprocal temperature for (a) BeF_2 and (b) SiO_2 with logarithmic scale on y-axis.

TABLE 1: Least Squares Linear Fits of $\ln A = 1000m_A/T + c$[a]

ρ (g cm^{-3})	T (K)	m_η	m_σ
1.5	2000−3000	12.4(5.2)	−8.1(1.6)
1.6	2000−3000	9.6(2.7)	−7.9(2.1)
1.7	2000−3000	12.1(6.7)	−7.4(5.4)
1.8	1750−3000	12.4(6.5)	−7.0(3.9)
2.0	1500−3000	7.4(3.8)	−5.8(5.1)
2.2	1500−3000	5.4(2.3)	−5.3(1.8)
2.4	1500−3000	4.9(2.8)	−4.6(3.9)
2.6	1500−3000	4.2(4.7)	−4.0(2.4)
2.8	1500−3000	4.0(4.0)	−3.4(4.4)
3.0	1500−3000	3.7(3.8)	−3.0(3.7)

[a] A is the shear viscosity, η or ionic conductivity, σ for BeF_2. The numbers enclosed in brackets are the respective % errors in the slopes.

TABLE 2: Least Squares Linear Fits in $\ln A = 1000m_A/T + c$, for SiO_2[a]

ρ (g cm^{-3})	T (K)	m_η	m_σ
1.8	4500−6000	41.0(4.3)	−19.8(13.4)
2.0	4500−6000	43.9(2.7)	−19.5(12.2)
2.2	4500−6000	41.5(5.7)	−22.3(9.9)
2.6	4250−6000	24.6(4.4)	−15.2(7.6)
3.0	4000−6000	16.1(3.2)	−13.3(3.8)
3.4	4000−6000	11.4(4.7)	−9.7(5.8)
3.8	4000−6000	12.7(5.4)	−8.9(6.6)
4.2	4000−6000	15.9(7.4)	−10.1(7.0)

[a] Details same as Table 1.

form over the temperature range from 4000 to 6000 K. Along low and intermediate density isochores, however, a deviation from linear behavior is seen for state points below the crossover temperature from normal to anomalous behavior ($T_{\mathrm{TMD}}^{\mathrm{max}}$) and the Arrhenius fitting is valid over a more limited temperature range. The validity of the Stokes−Einstein relation for these systems, discussed in greater detail below, implies that the temperature dependence of the self-diffusivities can be deduced from that of the viscosities.

We then consider the validity of the Arrhenius relationship for the conductivity, as shown in Figure 3. In the case of BeF_2, $\ln \sigma$ shows a linear dependence on $1/T$ over a temperature range from 1500 to 3000 K for isochores lying above 2.0 g cm^{-3}, but over a reduced temperature range for low densities. In the case of SiO_2, the quality of fitting of the σ data to the Arrhenius form is very similar to that seen in BeF_2 for the high-density regime above 2.6 g cm^{-3}. The deviations from the Arrhenius form for low-density isochores is much larger for SiO_2 than in the case of BeF_2, as indexed by the percentage error in the slopes of the linear fits to the form $\ln \sigma = 1000m_\sigma/T + c$.

3.2. Stokes−Einstein Relation. The Stokes−Einstein relation connects ionic diffusivities ($D_\pm$) with the viscosity (η):

$$D_\pm = k_B T/C\eta r_\pm \tag{3}$$

where r_+ and r_- are the cationic and anionic radii, respectively, and $C = 4\pi$ or 6π, depending on whether "slip" or "stick" boundary conditions, respectively, are used.[1] In this work, we compute $r_\pm$ assuming $C = 4\pi$. The Stokes−Einstein relation can be tested using diffusivity and viscosity data in a number of alternative ways. As a first test, we show in Figure 4 the relationship of the cationic and anionic diffusivities for the two melts. In the case of BeF_2, $D_+ = 0.78D_-$ and in the case of SiO_2, $D_+ = 0.79D_-$. It can be seen that the cationic and anionic diffusivities are linearly correlated, as expected from the

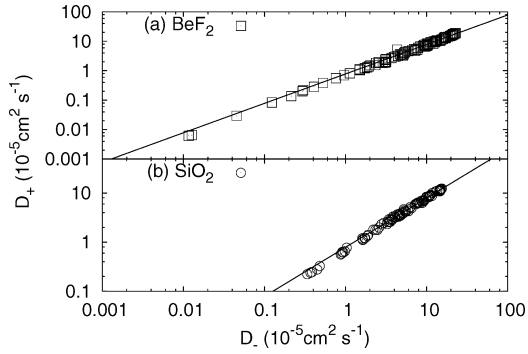

Figure 4. Correlation between cation and anion diffusivities for (a) BeF_2 (squares) and (b) SiO_2 (circles). The lines are $D_{Be} = 0.78D_F$ and $D_{Si} = 0.79D_O$.

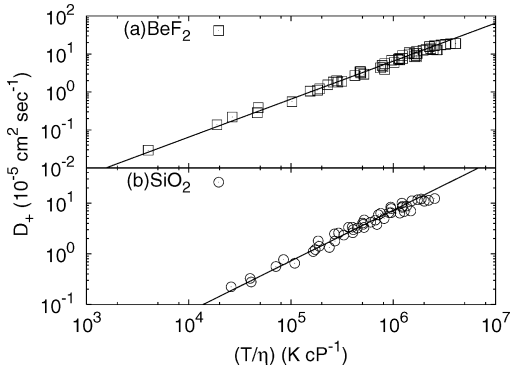

Figure 5. Logarithm of cationic diffusivities, ln D_+, as a function of T/η for (a) BeF_2 and (b) SiO_2. The straight line in part a is $\ln(D_+) = 0.95\ln(T/\eta) + \ln(k_B/4\pi r_+)$ and in part b, it is $\ln(D_+) = 0.94\ln(T/\eta) + \ln(k_B/4\pi r_+)$.

Stokes−Einstein relation. Alternatively, one can plot ln D_+ as a function of ln(T/η), as shown in Figure 5. If the Stokes−Einstein relation is obeyed, then the slope should be unity and the intercept should be $-\ln(4\pi r_+)$. Fractional Stokes−Einstein relations should give rise to slopes less than unity. In the case of BeF_2 and SiO_2, we observe slopes of 0.95 and 0.94, respectively.

The results shown in Figure 4 imply that the ratio of effective radii of cations to anions, given by $r_+/r_- = D_-/D_+$ remains constant over the range of state points studied. However, there are small but signicant changes in the effective hydrodynamic radius which are masked by the logarithmic plot of shown in Figure 5. Figure 6 shows the effective hydrodynamic radius of the cation as a functions of density for several isotherms of BeF_2 and SiO_2. The location of the first peak of the cation−anion pair correlation function does not vary significantly with temperature and provides a convenient unit for r_{eff}. We note that these estimates of the hydrodynamic radius are associated with a significant degree of statistical noise since they represent the ratio of two transport quantities. Despite this limitation, the overall trends are interesting and very similar for the two systems. At high temperatures, the network character of the melts is insignificant and compression leads to reduction of the r_{eff} value from 1.6 to about 0.7 as the number density varies from 17 to 40 nm^{-3}. For isotherms at temperatures $T < T_{TMD}^{max}$, we find a nonmonotonic behavior of the $r_{eff}(\rho)$ curves. At very low densities, compression reduces r_{eff} until a number density of about 22 nm^{-3}. Subsequently, compression results in a rise in r_{eff} until a maximum value is reached at $\rho^* \approx 30$ nm^{-3}. The rise in r_{eff} is presumably due to an increase in network flexibility as the local tetrahedral decreases; at high compressions, however, this trend is reversed because packing effects become

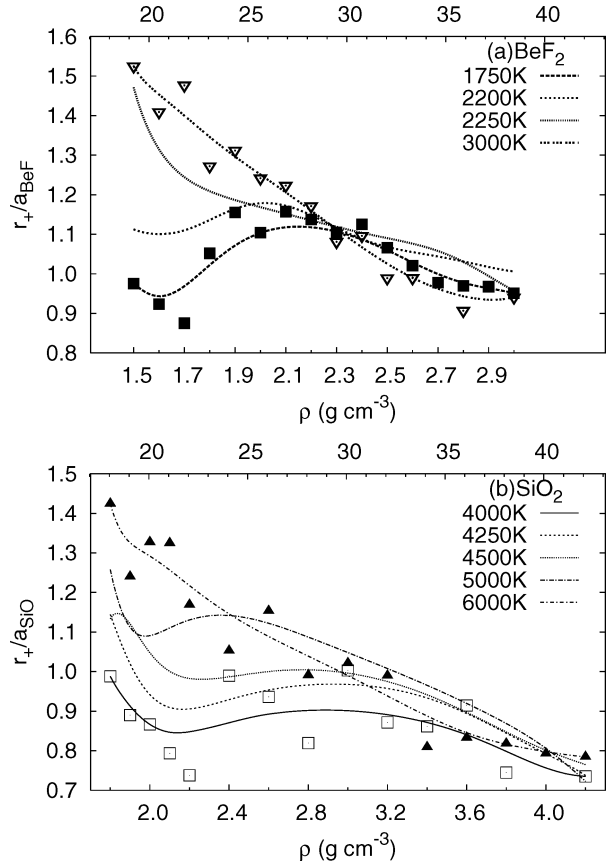

Figure 6. Effective hydrodynamic radius, r_{eff}, for the positive ion as a function of density for different isotherms of (a) BeF_2 and (b) SiO_2. The radius is scaled by the position of the first peak in the $g_{AB}(r)$, given by $a_{BeF} = 1.55A$ and $a_{SiO} = 1.6A$. Given the statistical noise in the r_{eff} estimate, the curves were generated by Bezier smoothing of the data. The actual data points are shown for the highest (triangles) and lowest (squares) temperature isotherms.

more important. It is also evident that decreasing temperature and the associated thermal fluctuations in the network structure, reduces the effective hydrodynamic radius. This is consistent with the results of earlier studies which use power spectral analysis to characterize network dynamics.[56]

3.3. The Nernst−Einstein Relation. The Nernst−Einstein equation relates the ionic diffusivities ($D_\pm$) to the ionic conductivity (σ):

$$\sigma = (e^2\rho/k_BT)(x_+z_+^2D_+ + x_-z_-^2D_-)(1 - \Delta) \qquad (4)$$

where e is the electronic charge, $x_\pm$ and $z_\pm$ are the ionic mole fractions and charges respectively and Δ is the Nernst−Einstein deviation factor.[1] Positive values of the Nernst−Einstein parameter are associated with a decrease in conductivity due to cooperative effects. The alkali halides typically have a Δ value of ∼0.3 due to a decrease in conductivity because of ion pair formation.[1] In the absence of collective effects, the ionic conductivity and diffusivity should show similar trends in density and temperature dependence. Figure 7 shows that both SiO_2 and BeF_2 show a sharp decrease in Δ as the extent of network formation becomes more pronounced in the anomalous regime. It is evident that for isotherms with $T < T_{TMD}^{max}$, the $\Delta(\rho)$ curves have well-defined maxima; a shallow minimum is also seen at high densities in the lowest temperature isotherms. Maxima in the $\Delta(\rho)$ isotherms occur at the same number

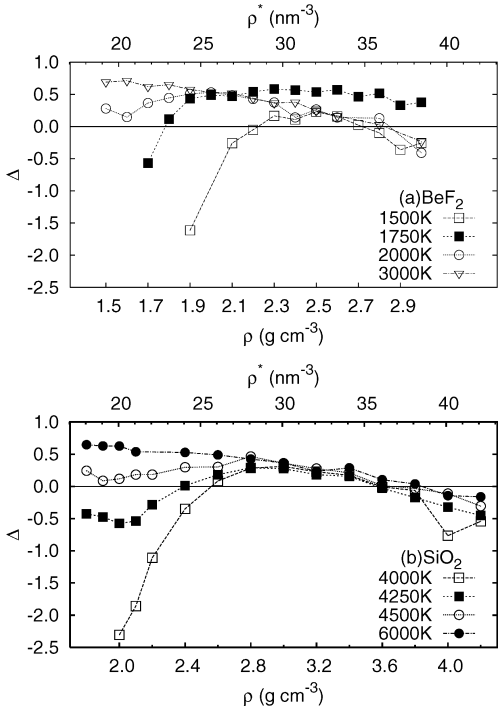

Figure 7. Nernst−Einstein deviation parameter as a function of density for various selected isotherms of (a) BeF_2 and (b) SiO_2. Note that number density (ρ^*) is also shown.

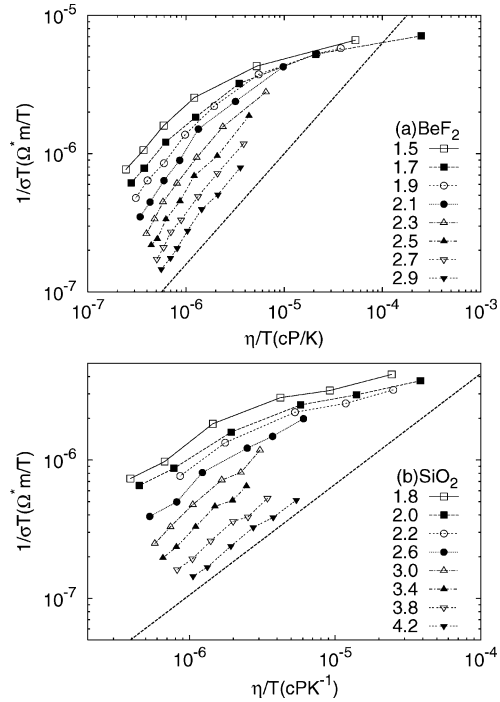

Figure 8. Variation of $1/(\sigma T)$ with η/T for selected isochores for (a) BeF_2 (b) SiO_2. Dashed lines indicate slope of 0.8.

densities for both ionic melts. Minima in the $\Delta(\rho)$ isotherms occur at 37 nm^{-3} for BeF_2 at 1500 K and 40 nm^{-3} for SiO_2 at 4000 K.

Deviations from the Nernst−Einstein relation in ionic melts have been previously discussed in the context of the glass transition. If both the Stokes−Einstein and the Nernst−Einstein relations are valid, then,

$$\sigma T = \left(\frac{e^2\rho}{4\pi}\right)\left(\frac{x_+ z_+^2}{r_+} + \frac{x_- z_-^2}{r_-}\right)(T/\eta) \qquad (5)$$

and $\ln(1/\sigma T)$ should be linearly dependent on $\ln(\eta/T)$ with a proportionality constant of unity.[61] In a study of ionic glass-formers, Voronel et al. found that all of the systems studied obeyed linear relationships with a slope of 0.8, where the intercepts depended on the precise chemical composition of the melt.[61] To our knowledge, however, none of the systems studied by them were network-forming melts. We show the analogous plots for SiO_2 and BeF_2 melts in Figure 8, noting that both systems are studied here in the liquid phase well above the glass transition. Since the both the systems show very similar behavior, we discuss only the behavior of the "Voronel" plot for silica. For densities above 2.6 g/cm^3, each isochore corresponds to a linear relationship between $\ln(1/\sigma T)$ and $\ln(\eta/T)$ with different intercepts for different densities. For lower density isochores, deviation from linearity is seen at low temperatures in the anomalous regime.

3.4. Excess Entropy Scaling of Transport Properties. In our previous work, we have demonstrated the validity of Dzugutov as well as Rosenfeld scaling for ionic diffusivities in silica and beryllium fluoride.[35,52] The ionic conductivities do not, however, scale with the excess or total pair correlation entropy but only with the cation−anion correlation contribution. Figure 9 shows the behavior of Rosenfeld-scaled viscosity, $\ln \eta^*$ versus the excess entropy, S_e, to illustrate the transition from high-temperature to low temperature behavior that was not discussed in our previous papers. Note that the thermodynamic excess entropy, and not the pair correlation entropy, is plotted in this figure. A linear relationship is observed between $\ln \eta$ and S_e for S_e values greater than $-3.5k_B$ for BeF_2 and $-4.5k_B$ for SiO_2. Below this value of S_e, the state points which belong to the lowest temperature isotherms lie on a straight line with a steeper slope. This type of a change in slope on the Rosenfeld-scaling plot has been observed earlier in the case of a supercooled Lennard−Jones liquid and associated with the onset of cooperative dynamics.[62] The present systems are studied at temperatures well above the glass transition temperature. It is possible, however, that the presence of a network, results in this change in Rosenfeld-scaling behavior at relatively high temperatures.

3.5. Relaxation Times. The dramatic breakdown of the Nernst−Einstein relation in the structurally anomalous region of the two tetrahedral melts suggests that the mechanisms of charge and momentum transfer must be very different in a network-forming ionic melt. In order to understand this further, we have examined the behavior of the autocorrelation functions (ACFs) in some detail. Figure 10(a) shows the charge flux ACF of BeF_2 melt at two state points. Figure 10(b) shows the corresponding pressure ACFs. Given that the pressure tensor is the negative of the stress tensor,[59] the pressure and stress ACFs will be identical. The charge-flux ACF decays much faster that the pressure ACF and has a pronounced oscillatory component. We found that the charge-flux ACFs for both BeF_2 and SiO_2 could be well-fitted by a function of the form $\exp(-t/\tau_\sigma)\cos(2\pi\nu t)$, where τ_σ is the associated relaxation time and ν is the frequency associated with the IR active local vibrational modes of the BeF_4^{2-} tetrahedra. In contrast, the pressure ACF displays no oscillatory component and decays very slowly, as illustrated in Figure 11. A convenient measure of the structural

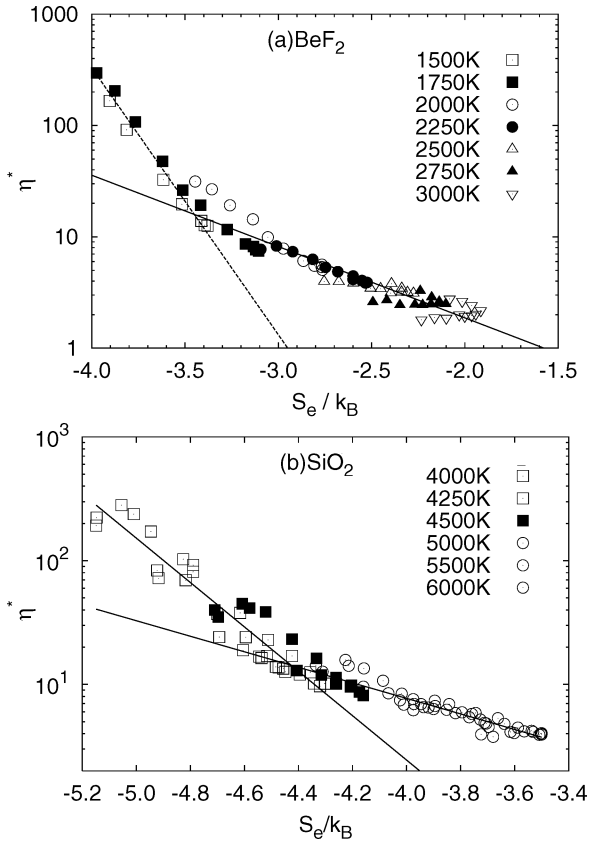

Figure 9. Rosenfeld-scaled viscosities (η^*) as a function of excess entropy, S_e for (a) BeF_2 and (b) SiO_2. The dimensionless diffusivity, $\eta^* = \eta(\rho^*)^{-2/3}(k_BTm)^{-1/2}$ where m is mass and ρ^* is number density of AB_2 units. In the case of BeF_2, the slopes of the straight lines are -1.47 and -5.52 while for SiO_2, they are -1.44 and -4.13. Note that the excess entropies were determined using the procedure given in ref 44.

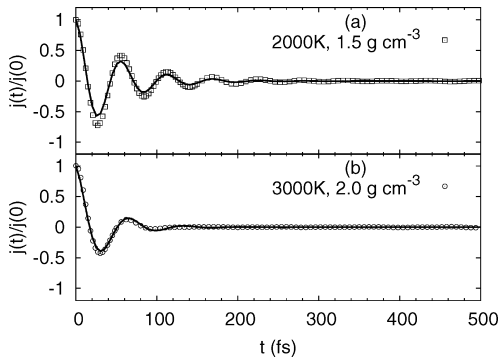

Figure 10. Normalized charge flux autocorrelation functions (points) for two state points: (a) (2000 K, 1.5 g cm^{-3}) in anomalous regime and (b) (3000 K, 2.0 g cm^{-3}) in normal regime. The solid lines show the fitting using the function $\exp(-t/\tau_\sigma)\cos(2\pi\nu t)$.

relaxation times associated with momentum transfer is therefore given by the Maxwell time, τ_M, defined as follows:

$$\eta(\tau_M)/\eta(\tau \to \infty) = 1 - (1/e) \qquad (6)$$

Figure 12 compares τ_M, τ_σ, and $\bar{\nu}$ for BeF_2; Figure 13 shows the analogous plots for SiO_2.

The frequency of the oscillatory component of the melts is temperature and density dependent. In the case of BeF_2, the frequency shifts from 600 cm^{-1} in the anomalous regime (low temperatures and low densities) to ~400 cm^{-1} in the normal regime. This is consistent with more precise estimates of the IR frequency obtained by Fourier transformation of the charge-flux ACF presented elsewhere.[58,63] In the case of SiO_2, the variation in frequency is less pronounced. For both melts, a strong correlation between viscosity and ν is observed, i.e., when the network-formation is pronounced, viscosity as well the frequency of the oscillatory component is large.

We now consider the relative magnitudes of relaxation times derived from the charge-flux and pressure ACFs. At high temperatures and densities when the ionic melt behaves es-

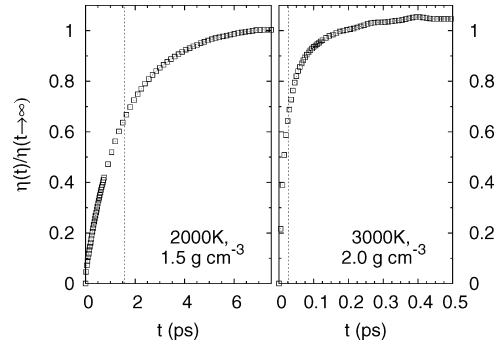

Figure 11. Time evolution of the integral of the stress tensor ACF, relative to its limiting value for two state points: (a) (2000 K, 1.5 g cm^{-3}) in anomalous regime (b) (3000 K, 2.0 g cm^{-3}) in normal regime. Vertical lines mark $t = \tau_M$.

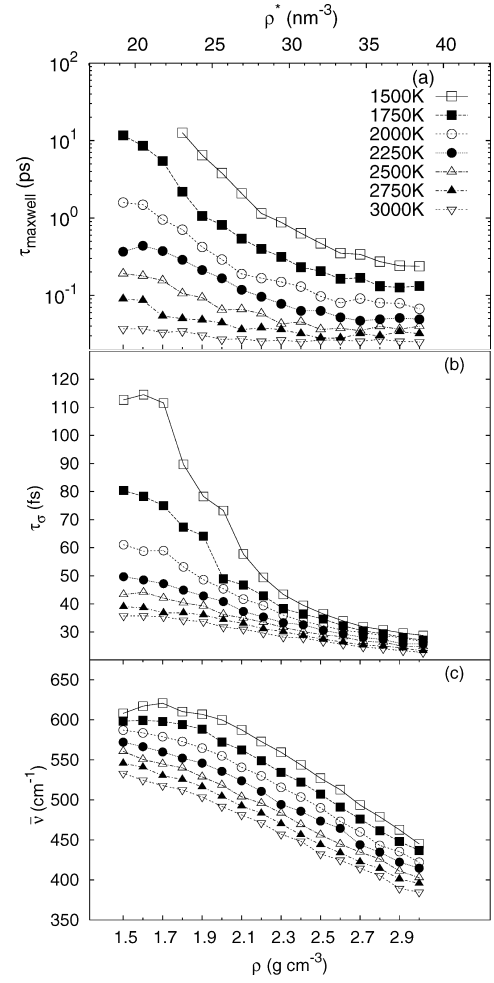

Figure 12. Density-dependent variation in BeF_2 of the following: (a) characteristic relaxation time of the pressure ACF, τ_M, given in ps; (b) characteristic relaxation time, τ_σ (in fs), of the charge flux ACF and (c) the characteristic oscillatory frequency of the charge ACF, $\bar{\nu}$.

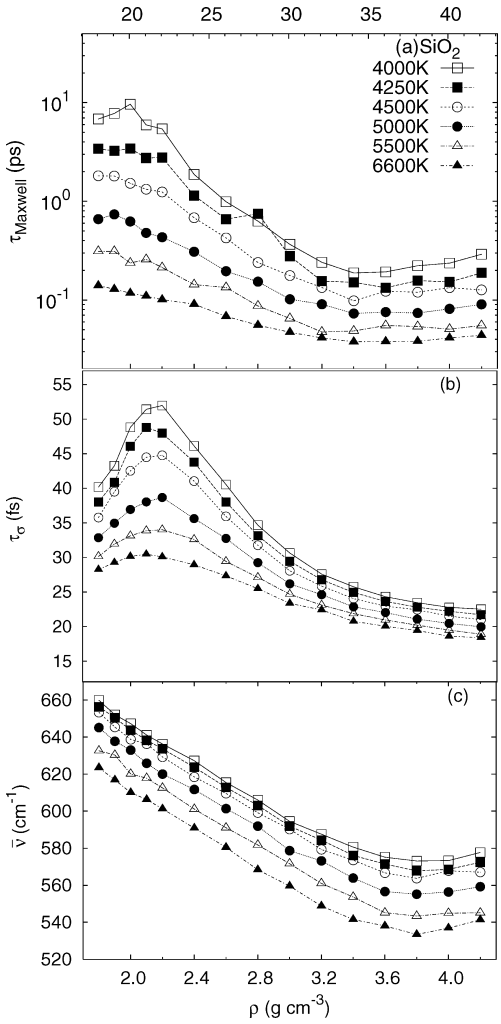

Figure 13. Density-dependent variation in SiO_2 of the following: (a) characteristic relaxation time of the pressure ACF, τ_M, given in ps; (b) characteristic relaxation time, τ_σ (in fs), of the charge flux ACF, and (c) the characteristic oscillatory frequency of the charge ACF, $\bar{\nu}$.

sentially as a simple liquid, τ_σ and τ_M are very similar. For example, along the 3000 K isotherm of BeF_2, τ_M is ~0.025−0.037 ps or 25−37 fs, while τ_σ is 20−35 fs. As network formation becomes more pronounced in the anomalous regime, the Maxwell times representing structural relaxation associated with the fluid viscosity increase over 4 orders of magnitude. In contrast, the τ_σ extracted from the charge-flux ACF varies by a factor of about 2. Therefore, as the system becomes "more anomalous", the ratio of τ_M to τ_σ increases exponentially and results in the dramatic deviation from Nernst−Einstein behavior observed earlier. The short relaxation times associated with the charge-flux ACF are likely to be correlated with short-length scale structural changes. The linear relationship observed in our earlier work between ln σ and S_{AB}, the cation−anion correlation contribution to the excess entropy, could therefore indicate that the charge-flux ACFs are sensitive to reorganizations involving only the nearest-neighbor shells of the ions.

It is interesting to compare our observations of the relaxation times associated with charge and momentum transfer with the recent work of Lubchenko on charge and momentum transfer in supercooled melts. Ref 64 provides a theoretical framework for understanding the decoupling of time scales associated with charge and momentum transfer, as determined from ionic conductivity and viscosity data. The steep decrease in viscosity as the glass transition is approached is associated with the formation of cooperatively reorganizing regions (CRRs) associated. As the size of the CRRs increases, structural relaxation slows down very rapidly. Ionic conductivity, in contrast, is dominated by the fastest relaxing regions of a liquid. In our case, the ionic melts have been studied at temperatures well above the glass transition. If the temperatures are sufficiently high, then the two relaxation times are very similar. Network formation, however, appears to induce a certain degree of cooperativity which results in a decoupling of charge and momentum transfer time scales.

The contrasting behavior of two important collective properties of ionic melts, viscosity, and ionic conductivity, provides an interesting perspective on the relationship between static correlation functions and dynamical quantities. Previous work on approximate scaling principles for classical fluids suggests that different dynamical quantities display differing sensitivities to static pair and multiparticle correlations.[65,66] The diffusivity and viscosity in particular seem to be largely determined by the pair correlations and are insensitive to any other change in the underlying interactions. To our knowledge, ionic conductivity has so far not been considered in the context of scaling relationships and is shown here to be qualitatively different from the diffusivity and viscosity in the sensitivity of the underlying autocorrelation functions to the static pair correlations.

4. Conclusions

The diffusivity, viscosity, and ionic conductivity of BeF_2 and SiO_2 melts are computed over the structurally normal and anomalous regimes. Diffusivity and viscosity display the characteristic nonmonotonic behavior associated with water-like mobility anomalies. Deviations from Arrhenius behavior along isochores is observed for state points belonging to the anomalous regime. In contrast, the conductivity increases monotonically with isothermal compression over the same set of state points.

The Stokes−Einstein relation is shown to hold over the entire range of state points. The effective hydrodynamic radius shows small but significant variations due to thermal fluctuations, compression, and local tetrahedral order. In the normal regime, it decreases monotonically with isothermal compression. In the anomalous regime, at moderate temperatures, it shows a nonmonotonic behavior with an initial rise in compression as the tetrahedral network breaks down.

Unlike the Stokes−Einstein relation, the Nernst−Einstein relation is shown to break down in the anomalous regime. The dependence of the Nernst−Einstein parameter as a function of the number density shows a parallel behavior for BeF_2 and SiO_2, suggesting a common structural origin. As a further test of the relationship between the three transport properties, $\ln(1/\sigma T)$ was plotted as a function of $\ln(\eta/T)$, which should lead to linear behavior with unit slope in case both the Stokes−Einstein and Nernst−Einstein relations are valid. Our data showed a linear dependence with a slope of 0.8 for state points in the normal regime. Deviations from linearity occur with onset of network formation, indicating that the Nernst−Einstein relation is more sensitive to cooperative effects seen in network-forming melts than the Stokes−Einstein relation.

The present study examines the Rosenfeld-scaling of the viscosities with the thermodynamic excess entropy for both SiO_2 and BeF_2. A distinct change in slope of the ln η^* versus S_e/k_B plots is observed at low temperatures for both the systems, possibly due to onset of cooperative effects.

In an effort to address the underlying causes for the breakdown of the Nernst−Einstein relation, we have computed the relaxation times, τ_σ and τ_M, associated with the decay of the charge-flux and

pressure ACFs, respectively. We show that as the ionic melt becomes more "anomalous" as a consequence of network formation, τ_M increases much more rapidly than τ_σ, suggesting that the mechanism for charge transport is sensitive to only fast, and short-length scale, reorganizations of the liquids. This would imply that reorganizations within the nearest neighbor shell are critical for conductivity and would be consistent with earlier observations that $\ln \sigma$ scales linearly with S_{AB}, the cation−anion correlation contribution to the excess entropy.

Structure−viscosity−conductivity relationships are known to be important from the point of view of technological applications, such as development of amorphous electrolytes.[22] We hope that this study will serve as a useful benchmark for related AB_2 systems, such as $BeCl_2$, $ZnCl_2$, GeO_2, and $GeSe_2$. Anion polarizability is known to play a crucial role in effecting a transformation from a three-dimensional liquid-state network of corner-sharing tetrahedra to liquid-containing one-dimensional chains of edge-sharing tetrahedra.[24,25] The corresponding changes in the relationship between structure, entropy, and mobility should be interesting.

Some general trends that emerge from this study on the relationship between transport properties in network-forming ionic melts require further investigation. Ionic conductivity is a characteristic transport property of such systems, that has so far not been considered in the literature on scaling relationships for dynamical properties. Our results suggest that it behaves very differently from the two commonly studied transport properties, viscosity and diffusivity. The differences between charge and momentum transport for strongly networked liquids are unexpected and show some resemblance to the behavior of liquids close to the glass transition. Another respect in which a strongly networked liquid resembles a simple liquid under strong supercooling is the change in slope of the Rosenfeld-scaling plot for viscosity for low-temperature state points.

Acknowledgment. C.C. would like to thank J.F. Douglas and M. Wilson for comments on our work on ionic melts and M. Ranganathan for drawing attention to the work of Andersen and co-workers on approximate scaling principles for dynamical properties. This work was financially supported by the Department of Science and Technology, New Delhi. M.A. would like to thank the Indian Institute of Technology−Delhi for award of a Senior Research Fellowship. A.G. would like to thank the University Grants Commission, New Delhi for award of a Junior Research Fellowship.

References and Notes

(1) Hansen, J.-P.; McDonald, I. R. *Theory of Simple Liquids*; Elsevier Academic Press: Amsterdam, 2006.
(2) Madden, P. A.; Wilson, M. *J. Phys.: Condens. Matter* **2000**, *12*, A95.
(3) McMillan, P. F.; Wilson, M.; Wilding, M. C.; Daisenberger, D.; Mezouar, M.; Greaves, G. N. *J. Phys.: Condens. Matter* **2007**, *19*, 415101.
(4) Scala, A.; Starr, F. W.; Nave, E. L.; Sciortino, F.; Stanley, H. E. *Nature* **2000**, *406*, 166.
(5) Saika-Voivod, I.; Poole, P. H.; Sciortino, F. *Nature* **2001**, *412*, 514.
(6) Saika-Voivod, I.; Sciortino, F.; Poole, P. H. *Phys. Rev. E.* **2004**, *69*, 041503.
(7) Shell, M. S.; Debenedetti, P. G.; Panagiotopoulos, A. Z. *Phys. Rev. E.* **2002**, *66*, 011202.
(8) Wilson, M.; Madden, P. A.; Hemmati, M.; Angell, C. A. *Phys. Rev. Lett.* **1996**, *77*, 4023.
(9) Hemmati, M.; Angell, C. A. *J. Non-Cryst. Solids* **1997**, *217*, 236.
(10) Poole, P. H.; Hemmati, M.; Angell, C. A. *Phys. Rev. Lett.* **1997**, *79*, 2281.
(11) Saika-Voivod, I.; Sciortino, F.; Poole, P. H. *Phys. Rev. E.* **2000**, *63*, 011202.
(12) Ford, M. H.; Auerbach, S. M.; Monson, P. A. *J. Chem. Phys.* **2004**, *121*, 8415.
(13) Horbach, J.; Kob, W. *Phys. Rev. B* **1999**, *60*, 3169.
(14) Voigtmann, T.; Horbach, J. *J. Phys.: Condens. Matter* **2008**, *20*, 244117.
(15) Wright, A. C.; Clare, A. G.; Etherington, G.; Sinclair, R. N.; Brawer, S. A.; Weber, M. J. *J. Non-Cryst. Solids* **1989**, *111*, 139.
(16) Takada, A.; Richet, P.; Catlow, C. R. A.; Price, G. D. *J. Non-Cryst. Solids* **2007**, *353*, 1892.
(17) Hemmati, M.; Moyinihan, C. T.; Angell, C. A. *J. Chem. Phys.* **2001**, *115*, 6663.
(18) Brawer, S. A. *Phys. Rev. Lett.* **1980**, *46*, 778.
(19) van der Meer, J. P. M.; Konings, R. J. M. *J. Nucl. Mater.* **2007**, *360*, 16.
(20) Heaton, R. J.; Brookes, R.; Madden, P. A.; Salanne, M.; Simon, C.; Turq, P. *J. Phys. Chem. B* **2006**, *110*, 11454.
(21) Salanne, M.; Simon, C.; Turq, P.; Heaton, R. J.; Madden, P. A. *J. Phys. Chem. B* **2006**, *110*, 11461.
(22) Salanne, M.; Simon, C.; Turq, P.; Madden, P. A. *J. Phys. Chem. B* **2007**, *111*, 4678.
(23) Wilson, M.; Madden, P. A. *Phys. Rev. Lett.* **1998**, *80*, 532.
(24) Wilson, M.; Sharma, B. K.; Massobrio, C. *J. Chem. Phys.* **2008**, *128*, 244505.
(25) Sharma, B. K.; Wilson, M. *J. Phys-Cond. Matt.* **2008**, *20*, 244123.
(26) Micoulaut, M.; Cormier, L.; Henderson, G. S. *J. Phys.: Condens. Matter* **2006**, *18*, R753.
(27) Shanavas, K. V.; Garg, N.; Sharma, S. M. *Phys. Rev. B* **2006**, *73*, 094120.
(28) Debenedetti, P. G. *J. Phys.: Condens. Matter* **2003**, *15*, R1669.
(29) Mishima, O.; Stanley, H. E. *Nature* **1998**, *396*, 329.
(30) Angell, C. A.; Bressel, R. D.; Hemmati, M.; Sare, E. J.; Tucker, J. C. *Phys. Chem. Chem. Phys.* **2000**, *2*, 1559.
(31) Tanaka, H. *Phys. Rev. E.* **2002**, *66*, 064202.
(32) Errington, J. R.; Debenedetti, P. G. *Nature* **2001**, *409*, 318.
(33) Xu, L.; Buldyrev, S. V.; Angell, C. A. *Phys. Rev. E.* **2006**, *74*, 031108.
(34) Dzugutov, M. *Nature (London)* **1996**, *381*, 137.
(35) Sharma, R.; Chakraborty, S. N.; Chakravarty, C. *J. Chem. Phys.* **2006**, *125*, 204501.
(36) de Oliveira, A. B.; Franzese, G.; Netz, P. A.; Barbosa, M. C. *J. Chem. Phys.* **2008**, *128*, 064901.
(37) Mittal, J.; Errington, J. R.; Truskett, T. M. *J. Phys. Chem. B* **2006**, *125*, 076102.
(38) Mittal, J.; Errington, J. R.; Truskett, T. M. *J. Phys. Chem. B* **2006**, *110*, 18147.
(39) Errington, J. R.; Truskett, T. M.; Mittal, J. *J. Chem. Phys.* **2006**, *125*, 244502.
(40) Mittal, J.; Errington, J. R.; Truskett, T. M. *J. Phys. Chem. B* **2007**, *111*, 10054.
(41) Goel, T.; Patra, C. N.; Mukherjee, T.; Chakravarty, C. *J. Chem. Phys.* **2008**, *129*, 164904.
(42) Agarwal, M.; Sharma, R.; Chakravarty, C. *J. Chem. Phys.* **2007**, *127*, 164502.
(43) Agarwal, M.; Chakravarty, C. *J. Phys. Chem. B* **2007**, *111*, 013294.
(44) Sharma, R.; Agarwal, M.; Chakravarty, C. *Mol. Phys.* **2008**, *106*, 1925.
(45) Green, H. S. *The Molecular Theory of Fluids*; North-Holland, Amsterdam, 1952.
(46) Baranyai, A.; Evans, D. J. *Phys. Rev. A* **1989**, *40*, 3817.
(47) Laird, B. B.; Haymet, A. D. J. *Phys. Rev. A* **1992**, *45*, 5680.
(48) Rosenfeld, Y. *Phys. Rev. A* **1977**, *15*, 2545.
(49) Rosenfeld, Y. *Chem. Phys. Lett.* **1977**, *48*, 467.
(50) Rosenfeld, Y. *J. Phys.: Condens. Matter* **1999**, *11*, 5415.
(51) Samanta, A.; Ali, S. M.; Ghosh, S. K. *Phys. Rev. Lett.* **2001**, *87*, 245901.
(52) Agarwal, M.; Chakravarty, C. *Phys. Rev. E.* **2009**, *79*, 030202.
(53) Woodcock, L. V.; Angell, C. A.; Cheeseman, P. *J. Chem. Phys.* **1976**, *65*, 1565.
(54) van Beest, B. W. H.; Kramer, G. J.; van Santen, R. A. *Phys. Rev. Lett.* **1990**, *64*, 1955.
(55) Kramer, G. J.; Farragher, N. P.; van Beest, B. W. H. *Phys. Rev. B* **1991**, *43*, 5068.
(56) Sharma, R.; Mudi, A.; Chakravarty, C. *J. Chem. Phys.* **2006**, *125*, 044705.
(57) Smith, W.; Yong, C. W.; Rodger, P. M. *Mol. Simulat.* **2002**, *28*, 385.
(58) Agarwal, M.; Chakravarty, C. *J. Chem. Sci.*, (accepted).
(59) Allen, M. D.; Tildesley, D. J. *Computer Simulation of Liquids*; Clarendon Press: Oxford, 1986.
(60) Frenkel, D.; Smit, B. *Understanding Molecular Simulation: from Algorithms to Applications*; Academic Press: London, 2002.
(61) Voronel, A.; Veliyulin, E.; Machavariani, V. S.; Kisliuk, A.; Quitmann, D. *Phys. Rev. Lett.* **1998**, *80*, 2630.
(62) Kaur, C.; Harbola, U.; Das, S. P. *J. Chem. Phys.* **2005**, *123*, 034501.
(63) Boulard, B.; Kieffer, K.; Phifer, C. C.; Angell, C. A. *J. Non-Cryst. Solids* **1992**, *140*, 350.
(64) Lubchenko, V. *J. Chem. Phys.* **2007**, *126*, 174503.
(65) Young, T.; Andersen, H. C. *J. Chem. Phys.* **2003**, *118*, 3447.
(66) Young, T.; Andersen, H. C. *J. Phys. Chem. B* **2005**, *109*, 2985.

JP903694B